Characterization of wave propagation in elastic and elastoplastic granular chains

Raj Kumar Pal
Department of Mechanical Science and Engineering, University of Illinois at Urbana-Champaign, Urbana, Illinois 61801, USA

Amnaya P. Awasthi and Philippe H. Geubelle*
Department of Aerospace Engineering, University of Illinois at Urbana-Champaign, Urbana, Illinois 61801, USA
(Received 7 October 2013; published 24 January 2014)

For short duration impulse loadings, elastic granular chains are known to support solitary waves, while elastoplastic chains have recently been shown to exhibit two force decay regimes [Pal, Awasthi, and Geubelle, Granular Matter **15**, 747 (2013).]. In this work, the dynamics of monodisperse elastic and elastoplastic granular chains under a wide range of loading conditions is studied, and two distinct response regimes are identified in each of them. In elastic chains, a short loading duration leads to a single solitary wave propagating down the chain, while a long loading duration leads to the formation of a train of solitary waves. A simple model is developed to predict the peak force and wave velocity for any loading duration and amplitude. In elastoplastic chains, wave trains form even for short loading times due to a mechanism distinct from that in elastic chains. A model based on energy balance predicts the decay rate and transition point between the two decay regimes. For long loading durations, loading and unloading waves propagate along the chain, and a model is developed to predict the contact force and particle velocity.

DOI: 10.1103/PhysRevE.89.012204 PACS number(s): 45.70.−n

I. INTRODUCTION

Granular media have potential applications in diverse fields involving dynamic wave propagation, ranging from impact wave shielding to determining mechanical properties of biological materials [1–3]. In the last few decades, extensive studies have been conducted on the distinct dynamic properties of these systems. Granular systems are typically composed of regular or irregular contacting granules [4–6] and have been extensively modeled as deformable spheres. Shock fronts [7] or wave trains [8] form under certain loading conditions.

Most of the studies in the literature have been conducted on nondissipative elastic spheres to characterize their response subjected to various loading conditions. Nesterenko [9] showed that a chain of unstressed elastic spherical granules in contact, subjected to an impulse load, transmits a compact stress wave called solitary wave, with features distinct from those of waves transmitted in precompressed chains. Wave trains in contacting elastic granules have been observed in various studies, starting from the works of Lazaridi and Nesterenko [8]. Job *et al*. [10] observed wave trains in granular chains subjected to impulse loadings in two cases: when the mass of the striker is large and when there is a change in radii along the chain. Sokolow *et al*. [11] conducted similar studies and noted the absence of a simple relationship between the amplitudes of various solitary waves in the wave train. Molinari and Daraio [7] studied the characteristics of periodic granular chains subjected to a constant velocity at one end and characterized the quasisteady response of the system using a homogenized equation and a traveling wave solution. In the first part of this work, wave propagation in monodisperse granular chains subjected to short and long duration force impulses is studied systematically. The peak contact force acting on a sphere and the leading wave velocity down a long chain are obtained. In the long duration case, bounds for the wave velocity are derived directly from the discrete governing equations, in contrast with the homogenized approximation or with the traveling wave approach followed by Molinari and Daraio [7].

In real systems subjected to high loads, point contacts between granules lead to stress concentrations causing plastic deformations, and the effects of plasticity become significant [12–14]. Pal *et al*. [12] modeled the effects of plasticity on wave propagation in granular chains and observed exponential and inverse force decay regimes along the chain. In other studies on dissipative elastic crystals [15,16], the dissipation is associated with the relative motion between particles. Vergara [16] developed a dissipative model for viscoelastic spheres in contact by parametrizing the contact law to include contributions of viscoelasticity and dependence on the square of relative velocity of contacting spheres. In Ref. [15], Carretero-Gonzalez *et al*. modeled dissipation by adding a power law of relative velocities to the Hertzian law, with the power law exponent determined from experiments to fit the simulation data. A key observation from that study is the existence of secondary waves below a critical exponent.

Most of the studies on wave propagation in granular chains have been conducted on monodisperse elastic chains. Wave attenuation has also been observed in chains having varying radii, due to impedance mismatch along the chain [10,17,18]. Others [19,20] have focused on the dynamics of random contacting spheres and their force propagation, dispersion, and attenuation characteristics.

In the second part of this work (Sec. III), the peak contact force along an elastoplastic chain is characterized for a wide range of loading conditions. A simplified contact law is used which captures the phenomenology of nonlinear elastoplastic models [12,21] and the response is obtained for a wide range of material properties. Wave propagation and properties for both

*Mailing address: 306 Talbot Laboratory, 104 South Wright Street, Urbana, IL 61801 USA; geubelle@illinois.edu

short and long loading times are described and the expressions for the peak force are obtained from the governing equations using energy balance and quasisteady state considerations.

II. ELASTIC CHAINS

A. Problem setup

In this section, the dynamic response of a semi-infinite monodisperse elastic granular chain subjected to a force impulse at one end is studied. The granular chain is composed of spherical contacting beads. The dynamic response of this system can be modeled as a spring-mass system, with the spheres modeled as point masses and the contact between them represented by nonlinear springs. These nonlinear springs follow a contact law based on Hertzian theory for spherical surfaces in contact [22]. The equation of motion of the ith sphere is given by

$$m_i\ddot{u}_i = F_{i-1,i}(\alpha_{i-1,i}) - F_{i,i+1}(\alpha_{i,i+1}), \tag{1}$$

where m_i and u_i are the mass and displacement of sphere i, respectively, $F_{i-1,i}$ is the contact force between granule i and $i-1$ obtained from a contact law, and $\alpha_{i-1,i}$ is the relative displacement defined by

$$\alpha_{i-1,i} = \begin{cases} u_{i-1} - u_i & \text{if } u_{i-1} > u_i \\ 0 & \text{otherwise.} \end{cases} \tag{2}$$

The contact force between the elastic spheres is modeled by the classical Hertzian contact law [22].

For the first sphere, the equation of motion is

$$m_1\ddot{u}_1 = -F_{1,2}\left(\alpha_{1,2}\right) + f\left(t\right), \tag{3}$$

where $f\left(t\right)$ is the external force applied to the left of the first sphere and is given by

$$f(t) = \begin{cases} A & \text{if } 0 < t \leqslant T, \\ 0 & \text{otherwise.} \end{cases} \tag{4}$$

For a given amplitude A and loading time T, the total impulse is thus $I = AT$.

A fourth-order Runge-Kutta scheme is used to solve the system of coupled ordinary differential equations with a time step of 5×10^{-9} s. In all simulations, the radii of spheres are taken to be 4.76 mm and the material properties are chosen to correspond to brass, with density $\rho = 8500\ \text{kg/m}^3$, Young's modulus $E = 115$ GPa, and Poisson's ratio $\nu = 0.30$. Let $E^* = E/2(1-\nu^2)$ and $R^* = R/2$ be the effective stiffness and effective radii of two identical contacting spheres [22]. The solutions are presented hereafter in a nondimensional form, with the force and impulse normalized as

$$\tilde{F} = F/E^*R^{*2}, \tag{5}$$

$$\tilde{I} = I/E^*R^{*2}\tau, \tag{6}$$

where τ is the intrinsic time scale associated with the elastic sphere system,

$$\tau = \sqrt{\frac{\pi\rho R^{*2}}{4E^*}}. \tag{7}$$

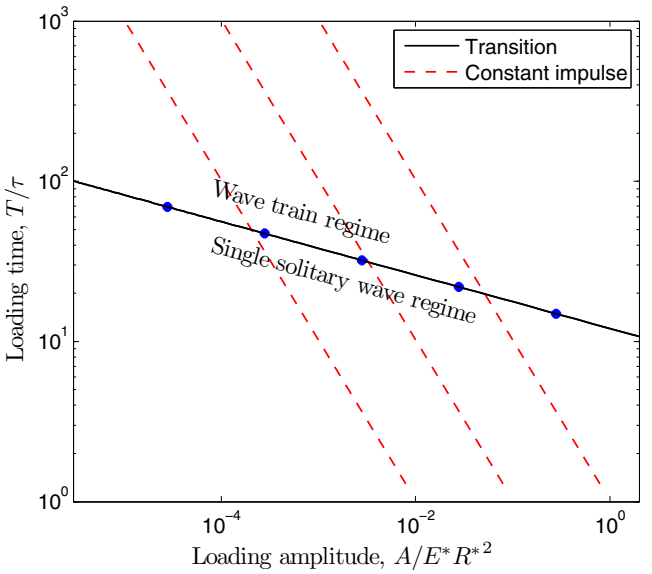

FIG. 1. (Color online) Transition from single solitary wave to wave train regime. The solid curve denotes the critical loading time above which wave trains form. This critical loading time follows a $-1/6$ power law with input amplitude. The symbols indicate numerical simulation values.

The key variables of interest are the peak contact force and wave velocity along the chain for a wide range of loading conditions.

B. Single solitary wave versus wave trains

To demonstrate the effect of loading times, the elastic chain is subjected to different load amplitudes A, with the total impulse kept fixed at $I = 0.40$ Ns. The loading times for the two cases are 1 μs ($T/\tau = 1.29$) and 100 μs $\left(T/\tau = 1.29 \times 10^2\right)$, respectively. Similar to the observations in Ref. [10], where a small (large) impact mass leads to a shorter (longer) loading time, for a fixed input impulse, a short loading time results in a single solitary wave, while a long loading time results in a train of solitary waves down the chain [8]. The leading solitary wave has the highest amplitude since the wave velocity depends on the force amplitude with 1/6 power [9].

A systematic study is conducted to determine the transition from a single solitary wave to a wave train. The loading amplitude A is kept fixed while the loading time T is increased from a low value until a transition time is attained when the response signal breaks into a train of solitary waves down the chain. The symbols in Fig. 1 show this transition time, obtained numerically for various loading amplitudes. Two distinct regimes exist and a power law with exponent $-1/6$ describes the transition. This implies that for any loading time T (or amplitude A), there is a transition amplitude A (or loading time T) below which a single solitary wave forms and above which a train of solitary waves forms.

We examined the contact force evolution with time at a few initial contacts along the chain for both the short $T = 1$ μs and long $T = 100$ μs duration loading cases. In the long loading duration case, the force evolution at a contact steepens down

the chain to form multiple distinct solitary waves, while in the short loading duration case, the contact time increases down the chain to form a single solitary wave. Due to the dependence of the wave speed on the force amplitude, there is an inherent time scale τ_s of loading at a contact for a solitary wave, which is a function of the amplitude. If the loading time at a contact is less than the time scale τ_s corresponding to the loading amplitude, the contact time increases and the amplitude decreases down the chain until a solitary wave forms, for which the contact time equals the inherent time scale τ_s corresponding to the loading amplitude at the contact. Similarly, if the contact time is longer than the time scale τ_s for the corresponding loading amplitude, the amplitude increases, the contact time decreases, and the wave breaks down the chain until a leading solitary wave forms. Thus, for a fixed input impulse, if the time of contact along the chain exceeds τ_s, the response breaks into wave trains, each having shorter contact time, and the peak force increases at contacts down the chain. On the other hand, if the time of contact is less than τ_s, the contact time increases and the peak force decreases as the wave progresses down the chain. The system has an inherent tendency to form solitary waves by appropriately adjusting the peak force and time of contact. Similar arguments have been made by Job *et al.* [10], who observed a transition depending on the size of the striker impacting the chain. Since the wave velocity scales with peak force amplitude as $F_p^{1/6}$, the inverse of time scale τ_s would also follow the same scaling law. Thus the transition time to wave trains T, which is the contact time at the first contact, also follows a $-1/6$ power law with loading amplitude, as seen earlier in Fig. 1.

C. Model

In this section, a model is developed to predict the peak contact force and leading wave velocity down an infinitely long chain, subjected to any constant loading amplitude and impulse. For sufficiently short loading times, the amplitude F_p of the solitary wave propagating down the chain depends only on the input impulse I. This amplitude can be evaluated by considering the limit of an infinite force acting for zero time. Indeed, the limiting case is equivalent to the problem of an initial velocity v_0 prescribed to the first sphere. Through dimensional arguments [2], the peak force of the solitary wave scales with initial velocity as $F_p \propto v_0^{6/5}$ and, from numerical experiments, the solution to this problem is determined to be

$$F_p = 0.719\left(m^3 E^{*2} R^* v_0^6\right)^{1/5} = 0.719\left(E^{*2} R^* \frac{I^6}{m^3}\right)^{1/5}. \tag{8}$$

Next, the response of the system is analyzed for large loading times. In this case, a train of solitary waves of decreasing amplitude traverses down the chain. Since the wave with the highest amplitude is the leading wave, the peak contact force down an infinite chain is the force due to the leading solitary wave. To determine this peak force, consider a chain subjected to a long loading time of $T = 10$ ms and $A = 40$ N. The contact force and sphere velocity distribution at time $t = 100$ ms are plotted in Fig. 2, showing two regimes: a constant force and velocity regime near the point of loading

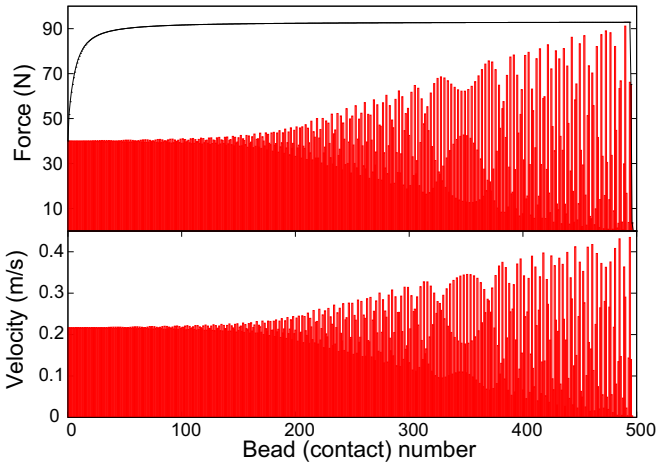

FIG. 2. (Color online) Contact force and bead velocity snapshots along the chain for a long loading time. Two regimes are seen: at the left end, the contact force and sphere velocity are constant, while at the right end, there are distinct waves. The solid curve in the top figure denotes the peak force achieved at every contact.

and a solitary wavelike regime at the leading edge. It is noted that there is a transition between the two regimes and the solitary waves at the leading front have not fully formed and started detaching yet. The waves at the leading front start to detach after loading stops, and we observe from numerical experiments that the peak force of the leading solitary wave is almost equal to the peak force at the leading front of the wave sufficiently down the chain. The solid curve in Fig. 2 shows the peak contact force, and although it continues to increase as noted in Ref. [9] for a related problem, the rate of increase is small and the peak force can be considered constant.

To determine the upper bound on the peak force, a simplified model is considered based on two regimes: a leading regime consisting of solitary waves and a trailing regime having a constant force and velocity with a sharp transition between them. In the trailing regime, the spheres move with a constant velocity v, and hence the bead displacement is given by

$$u(x,t) = U(x) + \left(t - \frac{x}{c_t}\right) v, \quad x < c_t t, \tag{9}$$

where c_t is the speed of the transition point and $U(x)$ is the bead displacement after the leading regime has passed x. Noting that the virial due to the above expression and in a solitary wave are constant, the kinetic K and potential P energy are related by the virial theorem as $4K = 5P$, which is found to be in excellent agreement with numerical simulations.

Let the leading front be moving with a velocity c and the solitary wave at the front have a corresponding peak contact force F_p. To evaluate the velocity of the spheres in the constant regime, we assume a quasisteady state of the front, wherein adjacent contacts have the same force histories, but are shifted by the time taken for the front to propagate a bead diameter. This leads to the following relation between the contact forces F_L and F_R acting on the left and right of a sphere, respectively:

$$F_R(t) = F_L\left(t - \frac{2R}{c}\right). \tag{10}$$

Integrating the equation of motion of the sphere and noting that $F_R(t) = F_L(t) = A$ when the bead is in the constant regime leads to the following relation for the bead velocity:

$$\int_0^\infty m\frac{dv}{dt}dt = \int_0^\infty (F_L - F_R)\,dt \tag{11}$$

$$\Rightarrow mv = \frac{2RA}{c}. \tag{12}$$

Finally, to evaluate the speed of the leading front, an energy balance in a time interval Δt leads to

$$Av\Delta t = \Delta P + \Delta K = \tfrac{9}{4}\Delta P. \tag{13}$$

Assuming that the force distribution and hence the energy in the solitary wave regime remain constant, all of the input energy in this time interval goes to the constant force regime. Since the contact force is constant in the first regime, Eq. (13) becomes

$$Av\Delta t = \frac{9}{4}\left(\frac{2A^{5/3}}{5k^{2/3}}\right)\frac{c\Delta t}{2R}, \tag{14}$$

where the bracketed term is the potential energy at a contact having a force amplitude A and $k = 4E^*\sqrt{R^*}/3$ is the constant defining the elastic contact. Using (12) leads to the following expression for an upper bound of the front velocity:

$$c^u = \sqrt{\frac{10A^{1/3}k^{2/3}D^2}{9m}}. \tag{15}$$

To evaluate a lower bound, consider the contact force acting on a spring between beads $i-1$ and i, given by Hertz law as

$$F = k\,(u_{i-1} - u_i)^{3/2}. \tag{16}$$

Differentiating (16), the relative velocity is given by

$$\dot{u}_{i-1} - \dot{u}_i = \frac{d}{dt}\left(\frac{F}{k}\right)^{2/3}. \tag{17}$$

Integrating (17) between $t = 0$ and $t \to \infty$ and again using quasisteady considerations, i.e., $v_i(t) = v_{i-1}(t - 2R/c)$, leads to

$$\frac{2vR}{c} = \left(\frac{A}{k}\right)^{2/3}. \tag{18}$$

Combining (12) and (18), we get a lower bound of velocity c of the front

$$c^l = \sqrt{\frac{A^{1/3}k^{2/3}D^2}{m}}. \tag{19}$$

The lower and upper values of wave speed given by the above expressions are $c^l = 668.0$ m/s and $c^u = 704.0$ m/s. Using Nesterenko's solution [9] for a solitary wave gives the upper and lower bound on peak force values, $F_p^u = 107.2$ N and $F_p^l = 78.15$ N. Comparing to the numerical values of wave velocity $c = 687.2$ m/s and peak force $F_p = 92.7$ N, we note a 3% and a 15% error in wave velocity and peak force, respectively. This difference arises due to the assumption that the entire energy input goes to the first regime. However, in numerical simulations, a careful observation reveals that the energy per unit length of chain is higher in the solitary wave regime than in the constant force regime, and there is a transfer of energy between the two regimes. Hence, the potential energy expression used in Eq. (14) is slightly lower than the total potential energy input to the system, and thus it is clear that the predicted force and wave velocity are indeed upper bounds on the exact values.

For long loading times leading to the formation of wave trains, the above analysis shows that the peak force of the leading solitary wave scales linearly with the input amplitude ($F_p \sim c^6 \sim A$), while in the single solitary wave regime, dimensional arguments show that the peak force scales with impulse as $F \sim I^{6/5}$. Figure 3(a) shows the variation of peak contact force ($\tilde{F}_p = F_p/E^*R^{*2}$) with loading amplitude ($\tilde{A} = A/E^*R^{*2}$) down a long chain for distinct impulses. Two

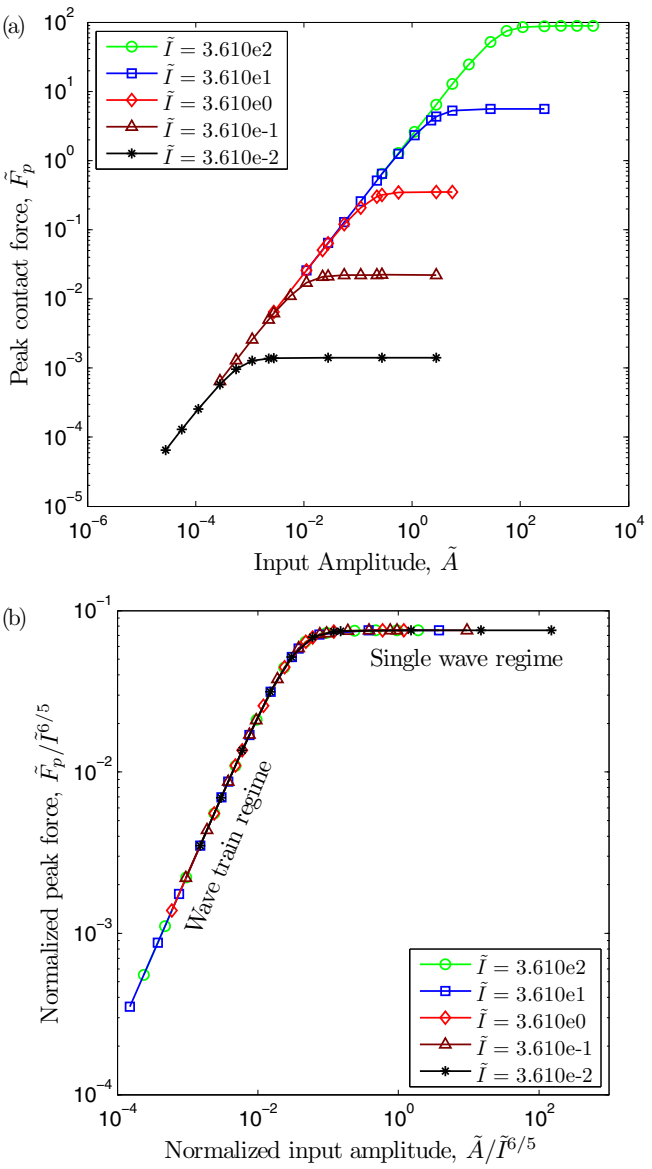

FIG. 3. (Color online) (a) Peak contact force for varying amplitudes and loading times, with each curve corresponding to a fixed impulse. (b) When normalized appropriately, the response collapses to a single curve. Two regimes are observed: the constant force corresponds to a single solitary wave, while the other regime corresponds to wave trains.

response regimes are observed: in the wave train regime, the peak force increases with amplitude of input force and is independent of I, while in the single solitary wave regime, the peak force is independent of the loading amplitude. Indeed, as observed in Fig. 3(b), the appropriate normalizations lead to the distinct responses collapsing to a single "master" curve. This normalized curve allows one to predict the peak contact force down a long elastic chain for any impulse, amplitude, and duration of step loading. For short loading times, the response is only a function of the form of the total impulse and does not depend on the form of the loading function, while for long loading times, the peak force is a function of loading amplitude only and independent of the loading duration or impulse.

III. ELASTOPLASTIC CHAINS

We now turn our attention to wave propagation in elastic-perfectly plastic granular chains for a wide range of loading durations. Two force-displacement models are considered in this work: the first is a simple bilinear model following Walton and Braun [23] and the second is a more accurate elastoplastic contact model due to Pal *et al.* [12]. Both models are shown in Fig. 4. The simpler bilinear model allows for the capture of the key contributions of the material-induced dissipation on the dynamic response of the elastoplastic chain, while the second, more complex contact model provides a more accurate quantitative description of the system, especially with regard to the elastic unloading and reloading. Two parameters define the bilinear model: the stiffness k associated with plastic loading and the unloading coefficient $\beta < 1$, which is the ratio of the residual displacement upon complete unloading to the maximum displacement previously achieved, i.e., the displacement at the start of unloading. The contact stiffness during unloading is the slope of the unloading curve $k_u = k/(1-\beta)$. The energy dissipated at a contact for which a peak force F has been attained is the difference in areas between the associated loading and unloading curves and is given by

$$E^{\text{dis}} = \int_0^{\alpha_{\max}} (F_{\text{load}} - F_{\text{unload}})\, d\alpha = \frac{F^2}{2}\left(\frac{1}{k} - \frac{1}{k_u}\right) = \frac{\beta}{2k(1-\beta)} F^2, \tag{20}$$

where $\alpha_{\max}$ is the maximum displacement corresponding to the force F. In this work, the plastic loading stiffness is set as $k = 18.5\sigma_y R^*$, with σ_y being the yield strength, to match the stiffness in plastic loading for large forces in the Pal model [12]. The dynamic response of a semi-infinite chain is studied for short and long duration loading times since, as demonstrated hereafter, the wave characteristics and contact forces along the chain are very different for these two loading conditions.

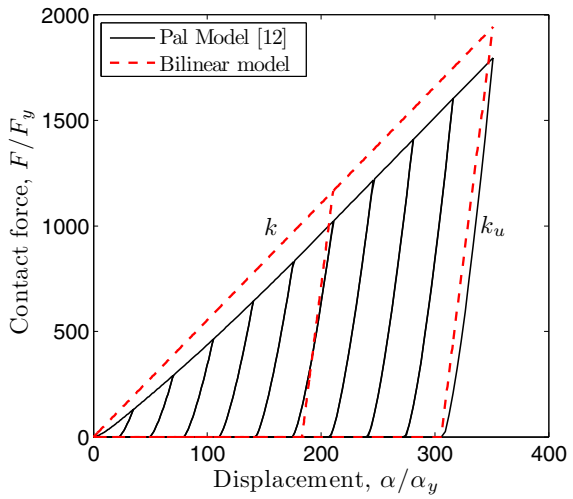

FIG. 4. (Color online) Two contact force-displacement laws for elastoplastic spheres. The simpler bilinear model is defined by two parameters: stiffness in plastic loading k and ratio of residual to maximum displacement, $\beta = 1 - k/k_u$. F_y and α_y denote the contact force and relative displacement at the onset of yield.

A. Short loading times

1. Wave characteristics

In this section, the contact force along the chain and its decay rate are characterized for the simpler, bilinear contact law. As shown in Pal *et al.* [12], for short loading times, elastoplastic chains have distinct characteristics, including wave merging and interaction, and rapid decay in peak force and energy dissipation along the chain. In that study, two regimes of spatial force decay were observed: exponential decay over the first few beads followed by an inverse decay. Furthermore, that study showed that after appropriate normalizations, the dynamic response of elastoplastic systems is identical for any impulse and short loading times.

The second regime of force decay starts when the trailing waves begin to cause dissipation at a contact, i.e., when the peak force due to the trailing wave is higher than the force previously attained due to the leading wave. Figure 5 shows the contact force and bead velocity history of the first few beads in an elastoplastic chain ($\beta = 0.80$) subjected to an impulse $I = 0.1$ Ns for a loading time $T = 1$ μs. For an elastic system subjected to such an impulse, the first few beads end up moving to the left following the initial impact events [24]. However, in the presence of plastic dissipation, we observe in Fig. 5(b) that the beads continue to move to the right. Due to higher stiffness and hence higher wave speeds during unloading, the decrease in contact force during unloading is much steeper than the increase during plastic loading [Fig. 5(a)]. This effect causes a lower impulse to be transmitted to the bead on the right. The momentum imparted to a bead, $mv = \int (F_L - F_R) dt$, is thus positive and the bead has a net residual velocity to the right after the leading wave has passed. Since there is energy dissipation at each contact, the net impulse transferred through the beads also decreases along the chain. Indeed, the residual velocity of beads and contact forces also decrease down the chain. As apparent in Fig. 5(b), the beads are initially in free flight and then collide, leading to secondary waves. This is in sharp contrast to the creation of secondary waves in elastic chains caused by wave steepening, as described previously in Sec. II B. Collisions between beads behind the leading wave cause contact forces, which can produce additional dissipation. To determine the point at which the transition happens, we first

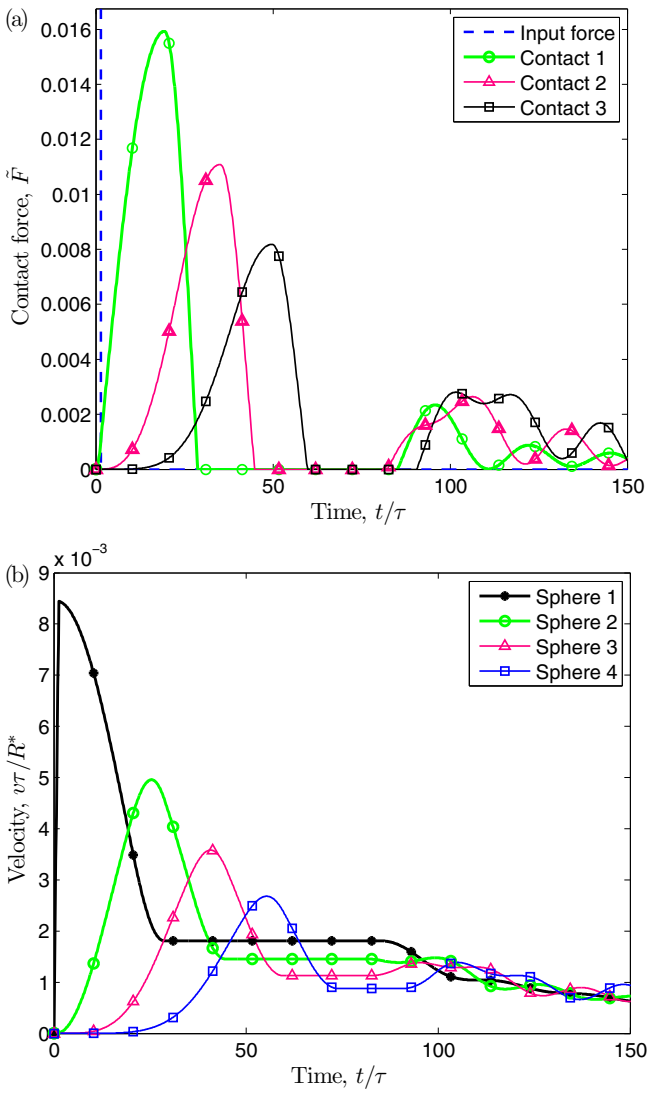

FIG. 5. (Color online) Time evolution of the contact force and bead velocity for the first few beads in an elastoplastic chain. Secondary waves behind the leading wave are caused by collisions of beads in free flight.

derive the spatial dependence of the peak contact force and residual velocity along the chain.

2. *Exponential decay regime*

In the first regime, a leading wave travels down the chain, causing an exponential decay in peak contact force. To derive the expression of that decay for the case of a bilinear elastoplastic contact law, we use an energy balance between the instants at which two adjacent contacts attain their respective peak force:

$$E_{\Delta t}^{\mathrm{dis}} = E_t^{\mathrm{tot}} - E_{t+\Delta t}^{\mathrm{tot}}, \tag{21}$$

where $E_{\Delta t}^{\mathrm{dis}}$ is the energy dissipated in a time interval Δt and E_t^{tot} is the sum of kinetic and potential energies over the entire chain at time t.

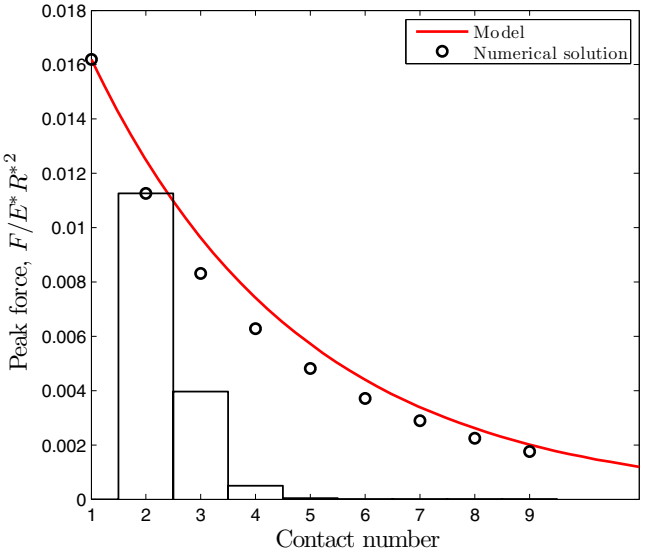

FIG. 6. (Color online) Force decay of the first few beads for short loading times. The peak force obtained numerically (circles) is well predicted by the analytical model (solid curve). Also shown is the leading wave profile (histogram) at the instant the second contact attains its peak force.

We now construct approximations for the various components of Eq. (21) as the leading wave propagates down the chain. At a contact, the potential energy is the area under the unloading curve and is a quadratic function of the force. Figure 6 shows the contact forces at the time instant when the second contact reaches its peak force. Let us assume that the leading wave has a self-similar structure, i.e., that the force at the contact ahead F_a is a fraction of the peak contact force ($F_a = \eta F$). Due to the bilinear nature of the contact law and the assumption of self-similar structure of the leading wave, the wave velocity, the time taken by the wave to traverse a bead, and thus the contact time T_c on a bead are constant. From dimensional arguments, the bead velocity v_m at the instant of peak contact force scales linearly with F, as $v_m/T_c \sim (F - F_a) \sim F$ and thus $v_m \sim F$. Similarly the free flight residual velocity v_r of the bead to the left of contact also scales as the peak contact force. Using the procedure described in the Appendix, the bead velocity v, contact force ahead F_a, and residual velocity of the bead v_r are related to the peak force F by

$$F_a = \eta F, \quad v_m = \gamma F, \quad v_r = \omega F, \tag{22}$$

where γ, η, ω are functions of material properties.

Though the leading wave spans four bead diameters and three contacts (Fig. 6), the contributions of potential energy due only to the two contacts having higher forces are considered to compute the total energy. Similarly, the velocity v_m of two beads whose contact force is maximum are considered for kinetic energy, while the remaining bead velocities and contact force, having small values, are neglected. When the force at a contact is maximum, the relative velocity of the beads at that contact is zero.

The total kinetic K and potential P energy components due to the leading wave are thus

$$K \approx 2\left(\frac{1}{2}\right) m v_m^2 = m\gamma^2 F^2, \quad P \approx \frac{1}{2k_u}(F^2 + \eta^2 F^2). \quad (23)$$

Let the peak contact force at two adjacent contacts distance x and $x + dx$ be F and $F + dF$, respectively, and let Δt be the time interval between the times when the two adjacent contacts attain their respective peak forces. The energy dissipated in the time interval Δt as the peak force is attained at two adjacent contacts is

$$E_{\rm dis}^{\Delta t} = \frac{1}{2}\left(\frac{1}{k_u} - \frac{1}{k}\right)[F^2 + (1+\eta^2)(2FdF + dF^2)]. \quad (24)$$

Substituting these expressions into the energy balance [Eq. (21)] and accounting for the kinetic energy due to residual velocity v_r leads to

$$[(dF)^2 + 2FdF]\left[\frac{1+\eta^2}{2k} + m\gamma^2\right] + F^2\left[\frac{1}{2}\left(\frac{1}{k} - \frac{1}{k_u}\right) + \frac{1}{2}m\omega^2\right] = 0. \quad (25)$$

Noting that energy dissipation takes place at discrete locations along the chain separated by a distance D, we obtain the following differential equation:

$$\left[\left(D\frac{dF}{dx}\right)^2 + 2DF\frac{dF}{dx}\right]\left[\frac{1+\eta^2}{2k} + m\gamma^2\right] + F^2\left[\frac{1}{2}\left(\frac{1}{k} - \frac{1}{k_u}\right) + \frac{1}{2}m\omega^2\right] = 0, \quad (26)$$

whose solution is

$$F(x) = \exp\left[\frac{-x}{D} + \frac{x}{D}\sqrt{1 - D\frac{\left(\frac{1}{k} - \frac{1}{k_u} + m\omega^2\right)}{\left(\frac{1+\eta^2}{k} + 2m\gamma^2\right)}}\right]. \quad (27)$$

Figure 6 shows the comparison between the numerical solution (symbols) and approximation [Eq. (27)] for the peak force along the initial part of the chain. The difference between the numerical solution and analytical approximation arises due to the assumption of self-similar wave structure, whereas in numerical simulations, the bead velocity and force at the contact ahead also exhibit small variations with time of loading. The difference between the predicted peak contact force and that obtained numerically is found to be around 10%.

3. *Transition and inverse decay regime*

The exponential decay regime ends when the contact force associated with trailing secondary waves is higher than that attained by the leading wave. As observed earlier (Fig. 5), secondary waves are caused by collisions of beads in free flight. From Eq. (22) and Fig. 5(b), we observe that the residual velocities of beads behind the leading wave scale with the peak force, and hence decrease down the chain. Eventually, these beads collide, causing secondary waves, which can be modeled as independent collisions between beads. To determine the peak force evolution of these secondary waves, we first determine the peak contact force between two beads in free flight having relative velocity Δv and operating in the elastic reloading regime of the force-displacement law. For the bilinear law, following Johnson [22], the relative displacement α satisfies the equation

$$m\ddot{\alpha} + 2k_u\alpha = 0, \quad (28)$$

and the peak contact force between them is given by

$$F_s = k_u\alpha = \sqrt{k_u m/2}\Delta v. \quad (29)$$

When two beads of equal masses following a nondissipative contact law collide, it is well known that their velocities interchange. Collisions between the beads in free flight lead to the contact forces in secondary waves, whose magnitude scales with the difference in velocities Δv. Since the residual velocity decreases down the chain ($v_t = \omega F$), this leads to a corresponding increase of the contact forces due to collisions, and a simple model is constructed to predict the peak force due to these collisions. Assuming that the collisions occur in order and are independent, the peak force due to secondary waves, based on Eq. (22), is given by

$$F_s^i = \sqrt{k_u m/2}\Delta v^i = \sqrt{\frac{k_u m}{2}}\frac{\Delta F^i}{\omega}, \quad (30)$$

where ΔF^i is the difference in peak force attained at the first contact and the $(i+1)$th contact.

The solid and dashed curves in Fig. 7 respectively show the approximate spatial variation of the leading (27) and secondary (30) waves for three distinct values of unloading coefficient β. The corresponding numerical values of the peak force are denoted by symbols. The intersections between these

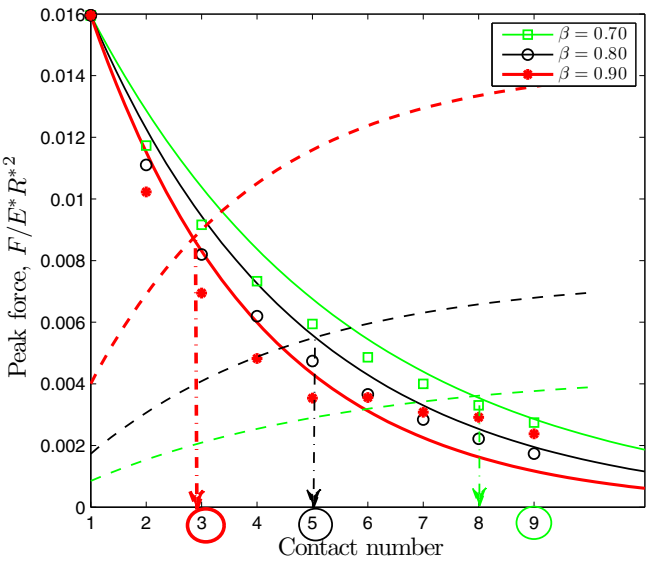

FIG. 7. (Color online) Spatial variation of peak contact force along the chain for three distinct unloading parameters β. The symbols denote numerical results, while the solid and dashed curves, respectively, show the decay predicted by the model [Eq. (27)] and the peak force due to secondary waves. Their intersection point (dotted vertical arrow) is the start of the transition from exponential to power law decay regimes. The circles on the x axis denote the transition points obtained numerically.

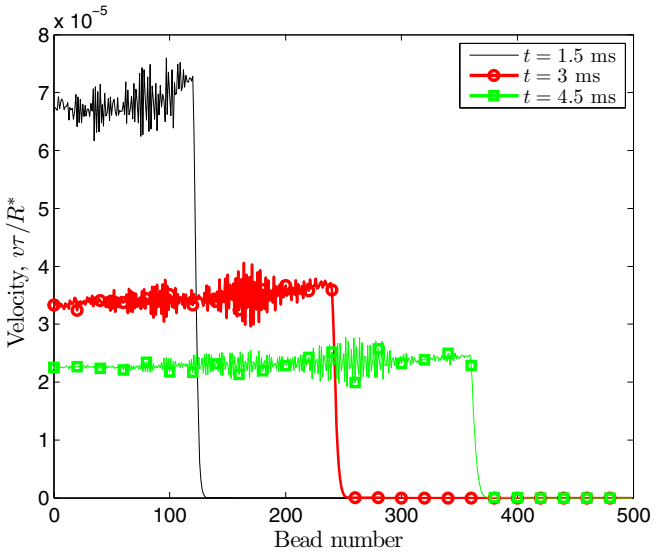

FIG. 8. (Color online) Bead velocity distribution along the chain at three time instants for a short loading time, $T = 1$ μs. In the inverse regime, the velocity distribution is almost uniform.

two sets of curves (emphasized by the dotted vertical arrows) provide estimates of the transition points between exponential and inverse decay regimes. For these three values of β, the numerical simulations give these transition points to be at the third, fifth, and ninth contact points, respectively, and are shown circled on the x axis in Fig. 7. These transition points are relatively well predicted by the model, with the difference due primarily to the assumption behind the prediction of the peak force of the leading wave.

As demonstrated in Ref. [12], the peak force decays inversely with distance in the second regime. Figure 8 shows the sphere velocity distribution along the chain in the inverse decay regime at three time instants for the bilinear material model with $\beta = 0.90$. As apparent there, the velocity distribution is almost uniform along the chain. Furthermore, from numerical simulations, we observe that most of the energy is associated with the kinetic energy of the spheres along the chain, while the total potential energy remains very small. A simple model based on energy balance is then constructed, assuming that the potential energy is negligible and that the velocity of spheres is uniform along the chain. The energy dissipated E_{dis} as the wave travels a distance Δx is then the difference in total kinetic energy,

$$E_{\text{dis}}(\Delta x) = \tfrac{1}{2} m v^2 \bar{x} - \tfrac{1}{2} m (v + \Delta v)(\bar{x} + \Delta \bar{x}), \qquad (31)$$

where $\bar{x} = x/D$ is the number of beads in a distance x. Using Eq. (20), assuming quasisteady conditions [Eq. (12)] in the time interval Δt and noting that the velocity in the loading regime $c = \sqrt{k/m}$ for the bilinear law, Eq. (31) simplifies to

$$\left(\frac{1}{k} - \frac{1}{k_u}\right) F^2 \Delta x = -\frac{F^2}{k}\Delta x - \frac{2F}{k} x \Delta F. \qquad (32)$$

Replacing the difference operators by differentials leads to

$$\frac{dF}{dx} + \left(\frac{1+\beta}{2}\right)\frac{F}{x} = 0, \qquad (33)$$

and its solution is given by

$$F = \left(\frac{a}{x}\right)^{(1+\beta)/2}, \qquad (34)$$

where a is a constant of integration. For values of β close to unity, the force is thus predicted to decay as an inverse power law with distance along the chain.

B. Long loading times

Finally, the behavior of elastoplastic chains subjected to impulses with long loading times and constant loading force is studied and expressions for the force and velocity of the system are developed. A monodisperse elastoplastic chain following a bilinear force-displacement law with unloading coefficient $\beta = 0.80$ is subjected to the loading conditions in Eq. (4) with loading time $T = 2.5$ ms and amplitude $A = 8$ kN. We first discuss the qualitative features of the wave structure and then construct a model for predicting the peak contact forces and particle velocities.

Figure 9 shows the distribution of contact force and bead velocity at three different time instants, along with the distribution of peak contact force attained along the chain. The distributions are seen to be qualitatively distinct at the three instants, having uniform values in certain regions with sharp transitions (wave fronts) along the chain. At early times ($t = 2$ ms in Fig. 9), when the chain is still under external loading, a single wave front travels to the right. After the loading stops ($t = 3$ ms), a trailing unloading wave travels from the left end. The beads behind this trailing wave have a lower velocity than the beads ahead of it, and the contacts have zero force behind the trailing wave front. As the force reduces from the constant value F_1 to zero in the contacts traversing the trailing wave front, these contacts operate in the steeper unloading part of the contact force-displacement law. Thus, this wave front has a higher velocity and eventually collides with the leading wave. After the collision of wave fronts, there is a decrease in the peak force of the leading wave and two wave fronts move in opposite directions, as shown by the results, corresponding to time $t = 5.2$ ms. The wave front traveling to the left is reflected at the free end and again travels to the right with the same amplitude, until it collides again with the leading wave front. This process continues indefinitely, with the trailing wave front being reflected from the free end and colliding with the leading wave front. The leading wave front always operates in the plastic loading part of the force-displacement law, while the trailing wave front always operates in the elastic unloading and reloading part. The amplitudes decrease progressively with each collision, as the energy gets distributed over a longer part of the chain. It is observed that the peak force in the first few contacts is higher than the constant value attained later. The peak force reaches a higher value than the amplitude A due to inertial effects in these contacts. In the remainder of this section, expressions for the steady contact forces and velocity of beads along the chain are derived and the point of transition when the wave fronts collide and the contact force drops is determined. In this work, the analysis is presented until the end of the first collision, although the procedure used here can be applied to determine the amplitudes after subsequent interactions.

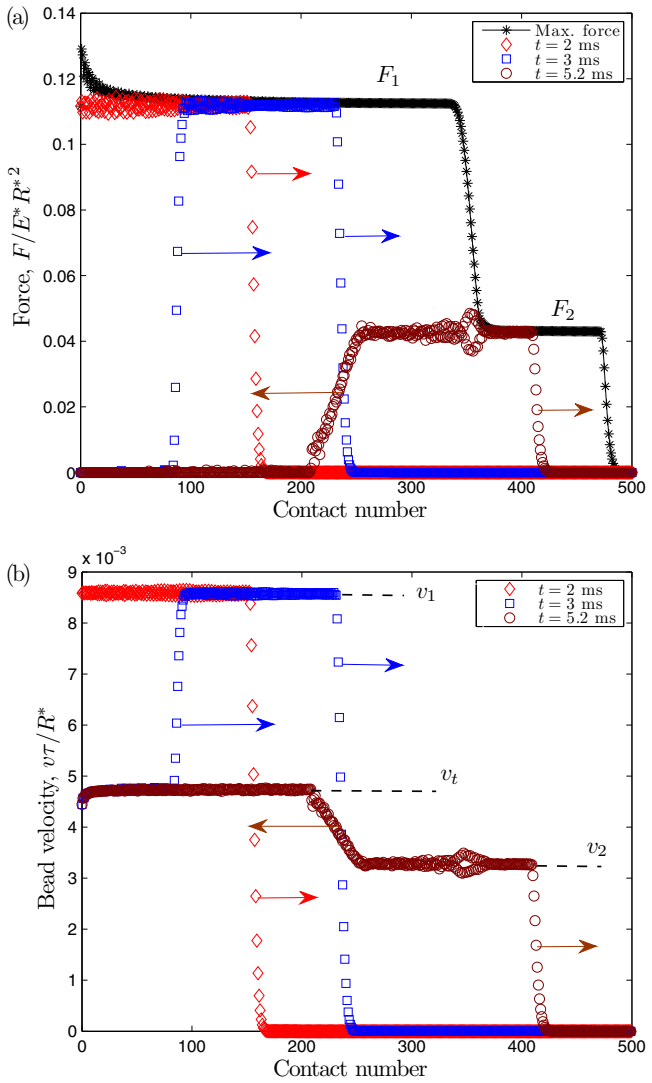

FIG. 9. (Color online) Force and velocity distribution along the chain for long loading time at three time instants. At $t = 2$ ms, a single wave moves to the right, while at $t = 3$ ms, two waves are moving to the right. Finally, at $t = 5.2$ ms, two waves are moving in opposite directions.

Along an elastoplastic chain following the bilinear law, the leading wave travels with a speed $c = D\sqrt{k/m}$ as it operates in the plastic loading regime of the force-displacement law. To evaluate the velocity of the beads, consider a bead down the chain, in contact with two beads, which exert contact forces $F_L(t)$ and $F_R(t)$ from the left and right side, respectively. Consider a time instant just after the leading wave has crossed this bead. The bead has attained a constant velocity v_1, and the left and right contacts have a constant force F_1. Similar to the elastic case, assuming a quasisteady response between two adjacent contacts, i.e., $F_R(t) = F_L(t - c/2R)$, and integrating the equation of motion until this time instant leads to the following relation for the bead velocity:

$$mv_1 = \frac{2F_1R}{c}. \tag{35}$$

After loading stops, a trailing wave starts from the first bead and merges with the leading wave. Since the beads in contact operate in the unloading regime as the trailing wave passes, the speed of the trailing wave c_u is given by the slope of the unloading curve in the force-displacement law and is higher than the leading wave velocity c. The trailing wave causes the contact forces to go down to zero behind it and the particle velocities go down to v_t. Again, integrating the equation of motion until a time instant just after the passage of this trailing wave gives the bead velocity in this region as $v_t = v_1 - 2F_1R/c_u$. The transition distance x_t and time T_t when the trailing wave merges with the leading wave are given by

$$x_t = T\left(\frac{1}{c} - \frac{1}{c_u}\right)^{-1}, \quad T_t = x_t/c. \tag{36}$$

The merging of leading and trailing waves leads to a decrease in the peak contact force and velocity of the beads, and two wave fronts move in opposite directions. The wave front moving to the right operates in the plastic loading regime, while the wave front moving to the left operates in the elastic reloading regime. It is noted that all of the beads are moving to the right, and the left wave front is formed by the collision of left beads with the right beads, which move with a lower velocity. Again, assuming a quasisteady state and integrating the equations of motion of two beads, one ahead of and the other behind the transition point from T_t until a time instant after the passage of both the wave fronts across these two beads, leads to

$$m(v_2 - v_t) = -F_2\frac{2R}{c_u}, \quad m(v_2 - 0) = F_2\frac{2R}{c_u}. \tag{37}$$

Solving the above system leads to the following expressions for the peak force and bead velocity:

$$F_2 = \frac{mv_t}{D}\left(\frac{1}{c} + \frac{1}{c_u}\right)^{-1}, \quad v_2 = v_t\left(1 + \frac{c}{c_u}\right)^{-1}. \tag{38}$$

Finally, it is noted that although the peak contact force in the first regime is a function of the unloading parameter β, the steady state force F_1 decreases gradually to reach the input amplitude A. Table I presents a comparison of various variables computed using the above expressions with values extracted from numerical simulations for a loading amplitude $A = 8$ kN and impulse $I = 20$ Ns. A good agreement is observed. This model can easily be extended to predict the peak force, wave, and particle velocity along the chain for any impulse and

TABLE I. Comparison of predicted values with numerical simulations for material with $\beta = 0.80$.

Variable	Numerical	Predicted
v_1 (m/s)	26.4	26.18
v_t (m/s)	14.6	14.47
v_2 (m/s)	14.5–15	14.84
F_2 (N)	3060	3056
x_t (m)	0.333	0.342

long times of loading, beyond the first interaction of wave fronts.

IV. CONCLUSIONS

In this paper, a systematic study has been performed on wave propagation in monodisperse semi-infinite elastic and elastoplastic chains subjected to short and long duration loadings, and expressions for the force and velocity of the wave have been determined using simple models and appropriate approximations. In the elastic case, the response is a function of the input impulse and time of loading. Two distinct regimes have been observed and identified, with the peak force of the leading solitary wave determined for both regimes. The analytical predictions have been found to be in good agreement with numerical simulations.

In elastoplastic granular chains, the mechanism of wave train formation is very distinct from its elastic counterpart. A simple bilinear model has been shown to capture the key phenomena associated with a more complex nonlinear model. The peak force decay rates in the exponential regime have been derived based on the bilinear model. Furthermore, the transition point has been predicted by determining forces due to secondary waves and compared with numerical simulations. The response is distinct for long loading times and a wave structure having a quasisteady front has been observed. The structure of the wave has been characterized using the quasisteady approximation and a simple model has been constructed to predict these quantities. The model predicts the contact force, wave, and particle velocity with good accuracy.

ACKNOWLEDGMENTS

The authors gratefully acknowledge the support of the United States Army Research Office through the Multi University Research Initiative Project No. W911NF0910436.

APPENDIX: LEADING WAVE STRUCTURE IN ELASTOPLASTIC CHAIN

To compute the total energy of the leading wave in the exponential decay regime, the velocities of the spheres supporting this wave and the contact forces between them (shown by histograms in Fig. 6) are determined in terms of the peak contact force F_p. All expressions are derived at the time instant a contact attains the peak force. The contact associated with the peak force and the contacts ahead operate only in the plastic loading regime and hence the contact forces and velocity of spheres are functions of k and m only and do not depend on the unloading law of the elastoplastic material. The expressions for F_p, the force on second contact F_2, and the velocity of the first two spheres v_m are derived by considering a series of linear spring mass system having mass m and stiffness k, respectively, and with the left end of the first mass subjected to an impulse I. They are given by

$$v_m = 0.482\frac{I}{m}, \tag{A1}$$

$$F_p = 0.721\sqrt{\frac{k}{m}}I, \tag{A2}$$

$$F_2 = 0.199\sqrt{\frac{k}{m}}I. \tag{A3}$$

The trailing wave velocity depends on the unloading coefficient β. The following relation is obtained for the trailing velocity v_t:

$$v_t = v_m - 0.599\sqrt{1-\beta}\frac{I}{m}, \tag{A4}$$

and is found to be in excellent agreement with the numerical values. Using the above relations, the maximum v_m and trailing v_t velocities of the two spheres and the contact force F_2 are expressed in terms of the peak contact force F_p in the leading wave.

[1] C. Daraio, V. F. Nesterenko, E. B. Herbold, and S. Jin, Phys. Rev. Lett. **96**, 058002 (2006).
[2] S. Sen, J. Hong, J. Bang, E. Avalos, and R. Doney, Phys. Rep. **462**, 21 (2008).
[3] V. F. Nesterenko, *Dynamics of Heterogeneous Materials* (Springer-Verlag, New York, 2001).
[4] C. Coste, E. Falcon, and S. Fauve, Phys. Rev. E. **56**, 6104 (1997).
[5] A. P. Awasthi, K. J. Smith, P. H. Geubelle, and J. Lambros, Mech. Mater. **54**, 100 (2012).
[6] A. Shukla, M. Sadd, Y. Xu, and Q. Tai, J. Mech. Phys. Solids **41**, 1795 (1993).
[7] A. Molinari and C. Daraio, Phys. Rev. E **80**, 056602 (2009).
[8] A. Lazaridi and V. Nesterenko, J. Appl. Mech. Tech. Phys. **26**, 405 (1985).
[9] V. Nesterenko, J. Appl. Mech. Tech. Phys. **24**, 733 (1983).
[10] S. Job, F. Melo, A. Sokolow, and S. Sen, Granular Matter **10**, 13 (2007).
[11] A. Sokolow, E. Bittle, and S. Sen, Europhys. Lett. **77**, 24002 (2007).
[12] R. K. Pal, A. P. Awasthi, and P. H. Geubelle, Granular Matter **15**, 747 (2013).
[13] E. Wang, P. Geubelle, and J. Lambros, J. Appl. Mech. **80**, 021009 (2013).
[14] E. Wang, T. On, and J. Lambros, Exper. Mech. **53**, 883 (2013).
[15] R. Carretero-Gonzalez, D. Khatri, M. A. Porter, P. G. Kevrekidis, and C. Daraio, Phys. Rev. Lett. **102**, 024102 (2009).
[16] L. Vergara, Phys. Rev. Lett. **104**, 118001 (2010).
[17] V. F. Nesterenko, C. Daraio, E. B. Herbold, and S. Jin, Phys. Rev. Lett. **95**, 158702 (2005).
[18] M. A. Porter, C. Daraio, E. B. Herbold, I. Szelengowicz, and P. G. Kevrekidis, Physica D **238**, 666 (2009).
[19] M. Manciu, S. Sen, and A. J. Hurd, Physica D **157**, 226 (2001).
[20] M. Manjunath, A. P. Awasthi, and P. H. Geubelle, Phys. Rev. E **85**, 031308 (2012).
[21] C. Thornton, J. Appl. Mech. **64**, 383 (1997).
[22] K. Johnson, *Contact Mechanics* (Cambridge University Press, Cambridge, UK, 1985).
[23] O. R. Walton and R. L. Braun, J. Rheology **30**, 949 (1986).
[24] A. Chatterjee, Phys. Rev. E **59**, 5912 (1999).